Circumstellar dust shells around oxygen–rich long–period variables

K. S. Jeong*, E. Sedlmayr
(Institut fr Astronomie und Astrophysik, TU Berlin, D-10623 Berlin, Germany)
J. M. Winters
(DEMIRM, UMR 8540, Observatoire de Paris, 61 av. de l'Observatoire, F–75014 Paris, France)

Introduction

More than 80 % of the mass returned to the interstellar medium emanates from circumstellar outflows generated by stars evolving along the Asymptotic Giant Branch (AGB) (Gehrz 1989). AGB stars are, therefore, the major source for the replenishment of the interstellar medium with processed material, in particular in the form of complex molecules and of dust particles. Consequently, they play a key role for the chemical evolution of interstellar media and stellar systems.

In carbon-rich situations, for which the chemistry is well known, mainly homogeneous amorphous carbon grains and also Polycyclic Aromatic Hydrocarbons (PAHs) are formed. The outflows from these C–rich AGB stars are now well described (e.g., Fleischer *et al.* 1995, Winters *et al.* 1995, Winters *et al.* 2000). In oxygen–rich situations, almost all carbon is locked up into the chemically inert CO molecule. Therefore, grains can only be formed from molecules containing the remaining oxygen and the less abundant elements, Fe, Si, Mg, S, Al, and Ti. A *heterogeneous* composition of the emerging dust component, with a core consisting of a high temperature condensate and a mantle composed of a variety of oxides, results in this case (Gail and Sedlmayr 1998a, 1998b).

Recently, the *first* time–dependent self–consistent models for dust forming *oxygen–rich* stars have been obtained, including an appropriate description of the heterogeneous dust formation process (Jeong *et al.* 1999, Jeong 2000). These models are determined by a combination of stellar properties (stellar luminosity $L_\star$, stellar mass $M_\star$, stellar temperature $T_\star$, abundances of the elements ε_i), pulsational period P and the amplitude of pulsation Δu). The corresponding results are in good agreement with the observed properties, e.g. mass loss rates and expansion velocities.

Dust Formation

Nucleation seeds: In order to determine the most likely primary condensation seed for oxygen–rich environments, nucleation rates J_* were calculated for the candidates in a $\rho - T$ plane, relevant for the inner region of a dust forming circumstellar shell. Contour plots of the resulting nucleation rates are shown in Fig. 1. for various seed nuclei, assuming chemical equilibrium in the gas phase. Though this assumption of chemical equilibrium

*Corresponding author. e-mail: jeong@alt.physik.tu-berlin.de

may be considered as highly unrealistic in pulsating situations, due to the large numerical expenditure, no consistent non–equilibrium chemical structure exists so far for Miras and LPVs.

Since Al_2O_3 is already stable at very high temperatures, it might be expected to be the first condensate in the cooling outflows of oxygen–rich stars (e.g. Kozasa and Sogawa 1999). However, using the thermodynamic functions resulting from *ab initio* calculations for the Al_2O_3 molecule, a calculation of the equilibrium concentrations shows, that this molecule is virtually not present in the gas phase (Chang *et al.* 1998, Patzer *et al.* 1999). Therefore, *homogeneous nucleation of molecular Al_2O_3 from the gas phase seems to be very unlikely in a circumstellar environment* and hereafter is considered only as growth species.

Although SiO is the most abundant candidate for nucleation in oxygen–rich circumstellar shells, its nucleation rate only peaks around 600 K, which is significantly lower than the typical temperatures at the inner edge of the dust shells as derived from infrared interferometry (Danchi *et al.* 1994). Efficient Fe nucleation occurs only at temperatures well below 1000 K. Only the titanium oxides show relevant nucleation rates at temperatures above 1000 K where TiO_2 nucleation is by far more efficient, due to its higher molecular concentration in the relevant region of $p - T$ plane.

Heterogeneous growth on TiO_2: The TiO_2 seed nuclei grow by accretion of those molecular species, which can form a stable condensate under the thermodynamic conditions prevailing in the circumstellar environment. The respective monomer of these condensates does not necessarily have to exist in the gas phase, but may be formed by chemical reactions on the grain surface from the atoms and molecules present in the gas phase. Actual formation of such a solid compound requires that all the generalized supersaturation ratios of the contributing atomic and molecular species are larger than unity (Dominik et al. 1993).

Results

The radial structures of the four dynamic models are depicted at the zero phase of a pulsation cycle, in Fig. 2 and the input parameters for model calculations are listed in Tab. 1.

Model	M_* [$M_\odot$]	T_* [K]	L_* [$L_\odot$]	C/O	Δu_p [km s^{-1}]	P [d]	$R_{*,0}$ [$R_\odot$]
A	1	2000	20 000	0.5	5	300	1176.0
B	1	2000	15 000	0.5	5	300	1018.7
C	1	2000	10 000	0.5	5	300	831.7
D	1	2000	8 000	0.5	5	300	743.9

Tab. 1 The input parameters for the model calculations.

Model	$\langle\dot{M}\rangle$ $[M_\odot\ yr^{-1}]$	$\langle u_\infty\rangle$ [km s^{-1}]	$\langle\rho_d/\rho_g\rangle$ $[10^{-3}]$	$L_{*,max}$ $[10^4\ L_\odot]$	$L_{*,min}$ $[10^4\ L_\odot]$
A	$6.2\,10^{-5}$	16.3	$4.2\,10^{-3}$	2.11	1.89
B	$2.7\,10^{-5}$	14.3	$4.1\,10^{-3}$	1.60	1.41
C	$3.6\,10^{-6}$	11.3	$3.9\,10^{-3}$	1.08	0.92
D	$4.2\,10^{-7}$	7.2	$3.2\,10^{-3}$	0.87	0.73

Tab. 2 The resulting wind properties from the extended models. These are given as time averaged values at $r = 35\ R_*$; mass loss rate $\langle\dot{M}\rangle$, the time averaged outflow velocity $\langle u_\infty\rangle$, the time averaged dust to gas ratio $\langle\rho_d/\rho_g\rangle$, the maximum and minimum luminosity $L_{*,max}$ and $L_{*,min}$ and the maximum velocity difference at the shock front Δu_{max}.

A direct comparison of the models shows the general characteristics of a close coupling of dust formation to hydrodynamics and to thermodynamics. The resulting wind properties are listed in Tab. 2.

- If the dust formation and growth is efficient, they induce a perturbation in the velocity structure which becomes a shock wave. Shock waves are passing periodically and propagate through the atmospheres of the models.
- The determining influence of the dust formation on the thermodynamical structure can be seen in the temperature structure between 2 R_0 and 4 R_0 which coincides with the first maximum of the radiative acceleration α. This temperature jump results from the opacity of the newly formed dust.
- The correlations among the number density of the dust grains per H–atom, the hydrodynamic structure, and the density are clearly to be seen. The radiation acceleration α correlates strongly with the mean radius $\langle r_d\rangle$ of the dust grains.
- The distribution of the dust particles is strikingly inhomogeneous, which can be seen from the number density of dust grains and the mean grain radius. The number density of the dust grains per H–atom $n_d/n_{<H>}$ shows a large variation, by three orders of magnitude, in the radial structure.
- The nucleation rates $J_*/n_{<H>}$ reach a maximum of several $10^{-20}s^{-1}$, but due to the constraint on the condensible TiO_2 molecule in the gas phase through the depletion of Ti, the nucleation occurs in several separate regions where the condensible TiO_2 molecules are available.
- The mean radius of the dust grain also reveals the inhomogeneity in the radial structure, and it shows a wide range of values between 0.01 μm and several 0.5 μm.

All models have in common the levitation of the atmosphere in comparison to an exponentially decreasing density structure of hydrostatic models. This effect is mainly due to the deposition of mechanical energy caused by the pulsation.

The degree of condensation f_{cond}: Fig. 3 depicts the degree of condensation $n_i/n_{<i>}$ for each element i contained in the dust grains in the radial structure. The degree of condensation is strongly correlated with the density structure, which reflects the dependence of the growth of dust grains on the density structure.

The growth species are mostly oxides of the less abundant elements, of which abundances are in general an order of magnitude smaller than the abundance of oxygen. Therefore, the amount of oxygen contained in dust grains is rather dependent on the amount of the less abundant elements in dust grains and the dust to gas ratio is essentially related to the total amount of the less abundant elements. Oxygen has a degree of condensation of $f_{cond} = 0.4$ which means that 40 % of the oxygen in gas is depleted and the rest of oxygen is mostly contained in the H_2O molecules of the gas.

The first depleted element from the gas phase is Al, followed by Ti. This is due to the high stability of the aluminium– and titanium–bearing species, e.g. Al_2O_3, Al_2SiO_4, Al_6SiO_{13}, Ti_2O_3 and $MgTiO_3$, even at higher temperatures (above 1 000 K). These two elements show complete depletion already at the inner region between 3 R_* and 4 R_*, just after the nucleation.

The degree of condensation for Mg, Si and Fe follows more or less a similar trend. For Mg and Fe, the degree of condensation reaches $f_{cond} = 1$ in several regions of the CDS, whereas Si is not completely depleted from the gas phase. The degree of condensation for Si generally varies between 0.7 and 0.85 The degree of condensation for Fe becomes remarkably larger after the temperature decreases below 1000 K. Sulphur generally has a lower degree of condensation than the other elements, but at temperatures lower than 600 K, its degree of condensation increases with increasing density profiles.

The Dust to gas ratio ρ_d/ρ_g: The radial structure of the dust to gas ratio ρ_d/ρ_g is shown in Fig. 4 at the zero phase of a pulsational cycle. The dust to gas ratio is given by

$$\frac{\rho_d}{\rho_g} = \sum_i \frac{\mathrm{m_i}}{\mu \mathrm{m_H}} f_c^i \varepsilon_i$$

where i labels elements with mass m_i, f_c^i is the degree of condensation of the respective element with an abundance ε_i and $\mathrm{m_H}$ is the mass of hydrogen atom. From the CO blocking, the abundance of available oxygen is taken as $\varepsilon_O^0 = \varepsilon_O - \varepsilon_C$.

It is interesting that the resulting dust to gas ratios ρ_d/ρ_g of all models are confined to a narrow interval between $3 \cdot 10^{-3}$ and $4.5 \cdot 10^{-3}$ which well agree with the observations (Knapp 1985, Sopka *et al.* 1985 Justtanont *et al.* 1994). In the oxygen–rich case this confinement of dust to gas ratio is due to the fact that the dust grains consist of the less abundant elements. The amount of dust is still small compared to the surrounding gas.

In comparison with the carbon–rich CDS, the dust to gas ratio is more or less in the same range, but the absorption by the dust grains is less efficient than by the carbonaceous dust grains. This effect of absorption by oxygen–bearing dust grains can be seen in the radial structure of acceleration ratio α.

Temporal variation of the mass loss rates: In Fig. 5, a temporal variation of the local mass loss rates at r= 35 R_* is depicted for model A during about 300 pulsation periods. The local mass loss rates show the regular temporal variation with the time step of about 20 P, which can reflect the passing–through time of the layered structure of dust shells at 35 R_*. The time step of the mass loss rates in Model B and C is longer than in case of Model A, 60 P and shows a distinct pattern of variation of the local mass loass rates as illustrated in Fig. 6 and Fig. 7.

References

Chang C., Patzer A. B. C., Sedlmayr E., Sülzle D., 1998, Eur. Phys. J. D **2**, 57

Danchi W. C., Bester M., Degiacomi C. G., Greenhill L. J., Townes C. H., 1994, AJ **107**, 1469

Dominik C., Sedlmayr E., Gail H.-P., 1993, A&A **277**, 578

Fleischer A. J., Gauger A., Sedlmayr E., 1995, A&A **297**, 543

Gail H.-P., Sedlmayr E., 1998, In Hartquist T., Williams D., *The Molecular Astrophysics of Stars and Galaxies*, p. 285, Oxford Science Pub., Oxford, GB

Gail H.-P., Sedlmayr E., 1998, In Sarre P., *Chemistry and physics of molecules and grains in space. Faraday Discussion no. 109*, p. 303, London, GB

Gehrz R. D., 1989, In Allarmandola L. J. and Tielens A. G. G. M., *Interstellar Dust*, p. 445, Kluwer Academic Pub., Dordrecht

Jeong K. S., 2000, *Dust shells around oxygen–rich Miras and long–period variables*, PhD thesis, Technische Universität, Berlin, FRG

Jeong K. S., Winters J. M., Sedlmayr E., 1999, In Le Bertre T., Lèbre A., Waelkens C., *IAU Symp. 191: AGB stars*, p.233 ASP Conf. Ser.

Justtanont K., Skinner C. J., Tielens A. G. G. M., 1994, ApJ **435**, 852

Knapp G. R., 1985, ApJ **293**, 273–280

Sogawa H., Kozasa T., 1999, ApJ **516** L000.

Patzer A. B. C., Chang C., Sedlmayr E., Sülzle D., 1999, Eur. Phys. J. D **6**, 57

Sopka R. J., Hildebrand R., Jaffe D. T., Gatley I., Roelling T., Werner M., Jura M., Zuckerman B., 1985, ApJ **294**, 242

Winters J. M., Fleischer A. J., Gauger A., Sedlmayr E., 1995, A&A **302**, 483

Winters J. M., Le Bertre T., Jeong K. S., Helling C., Sedlmayr E., 2000, A&A, in press

Acknowledgement: The calculations have been performed on the CRAY–computers of the Konrad–Zuse–Zentrum für Informationstechnik Berlin (ZIB).

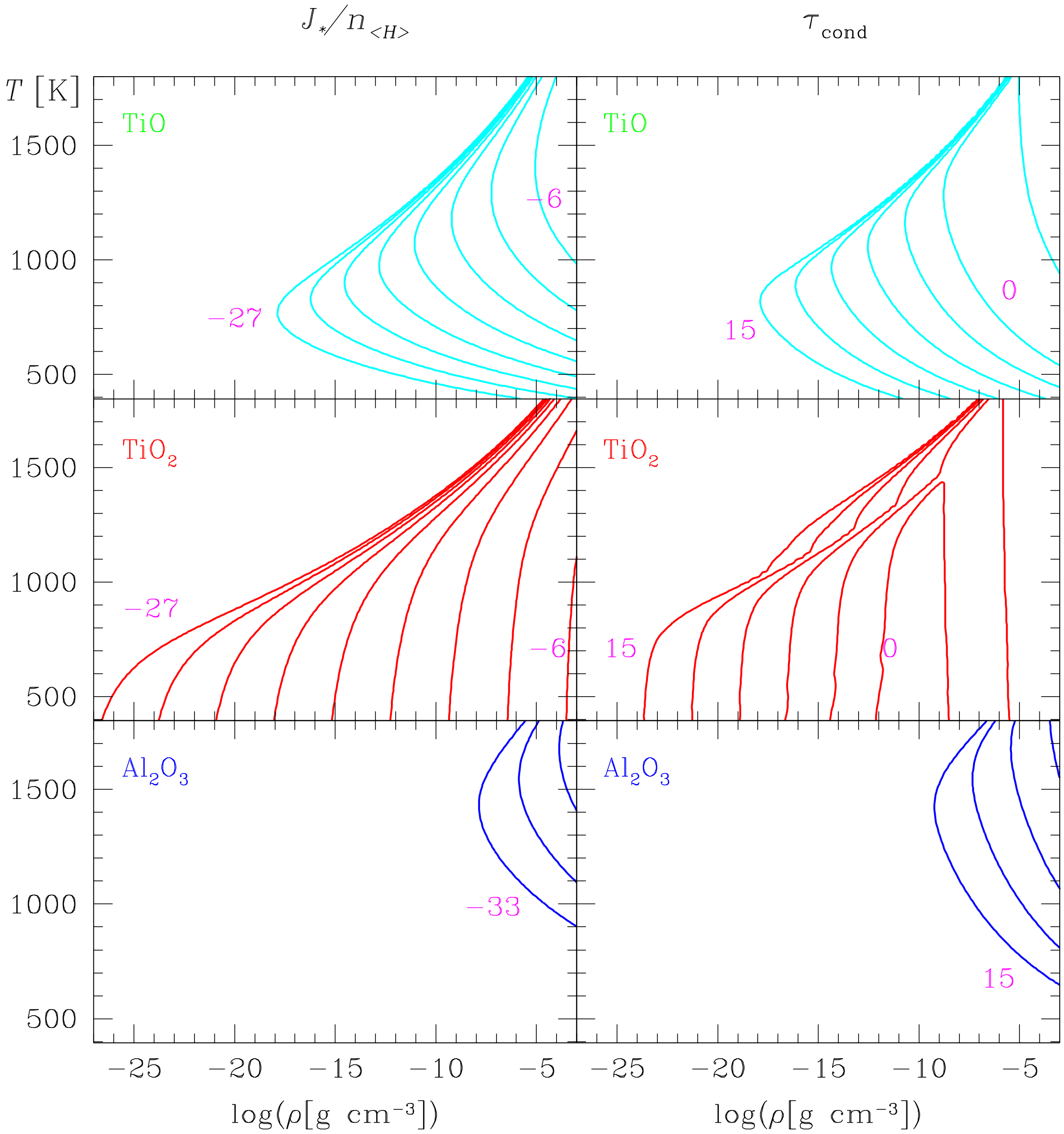

Figure 1: Contour lines of the nucleation rate for different nucleating species in the ρ–T plane. Contour levels are plotted in steps of $\Delta \log(J_*/n_{<\mathrm{H}>}) = 3$. τ_{cond} is the time in [s] needed that the condensing material is contained 10 % in the dust grains.

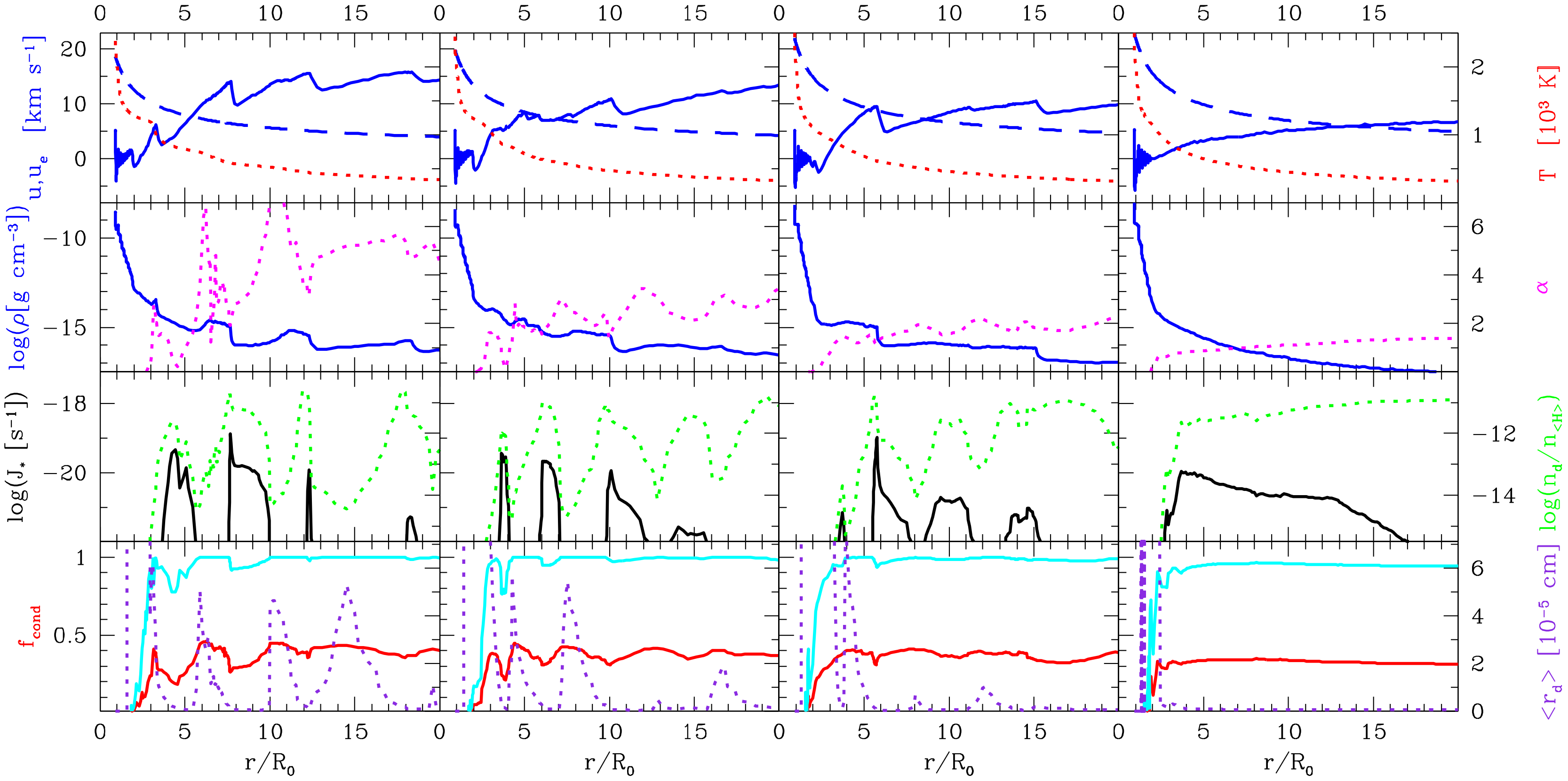

Figure 2: Radial structure of models A, B, C and D with $\Delta u_p = 5\,\mathrm{kms}^{-1}$ at the zero phase of a pulsational cycle. **upper diagram:** the velocity u (solid line) the escape velocity u_e (dashed line), both of which belong to the l.h.s. ordinate, and the temperature T (dotted line, r.h.s. ordinate); 2^{nd} **diagram:** the logarithm of the density ρ (solid) and the radiative acceleration α in unit of the gravitational acceleration (dotted); 3^{rd} **diagram:** the logarithm of the nucleation rate J_* (solid) and the logarithm of the number density of dust grains per H-atom $n_d/n_{<H>}$ (dotted); **lower diagram:** the degree of condensation for O (red solid), and Ti (lilac solid) and the mean grain radius $\langle r \rangle$ (dotted).

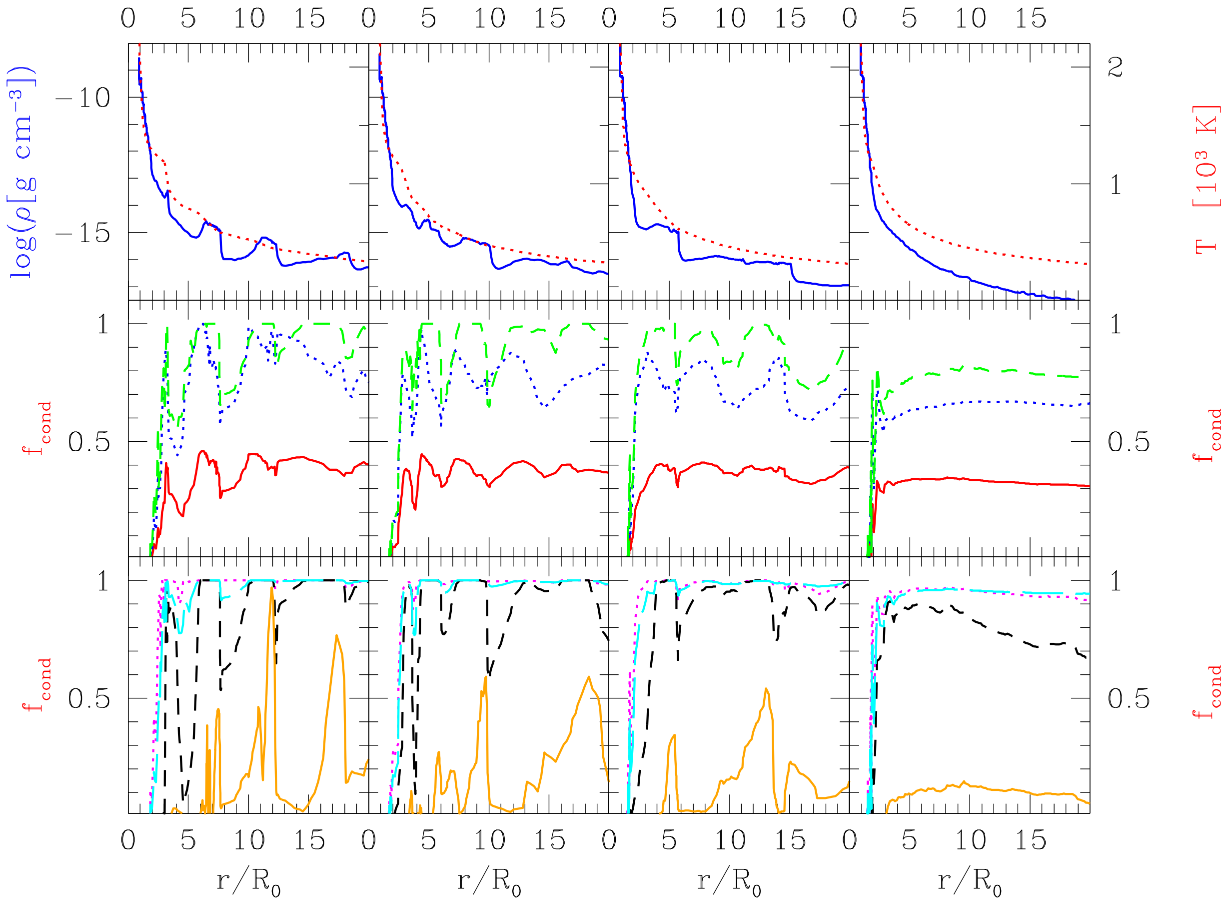

Figure 3: Radial structure of degree of condensation of elements for models with $\Delta u_p = 5\,\mathrm{km\,s^{-1}}$ at the zero phase of a pulsational cycle. The columns correspond to model A, B, C and D from left to right. **Upper diagram:** the logarithm of density ρ (solid) and the temperature T (dotted line); **middle diagram:** the degree of condensation for O (solid), Si (dotted line), and Mg (dashed line); **lower diagram:** the degree condensation of Al (dotted line), Fe (dashed line), S (dash-dotted line), and Ti (solid).

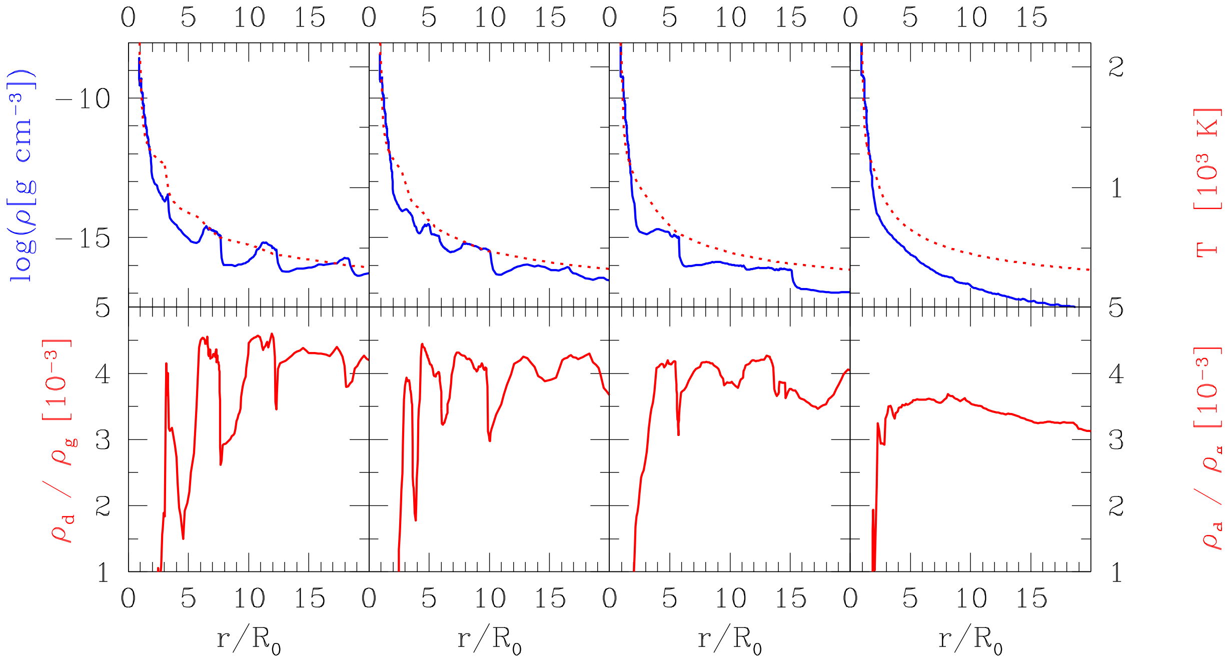

Figure 4: Radial structure of dust to gas ratio ρ_d/ρ_g for models with $\Delta u_p = 5\,\mathrm{km\,s^{-1}}$ at the zero phase of a pulsational cycle. The columns from left to right correspond to Model A, B, C and D, respectively.

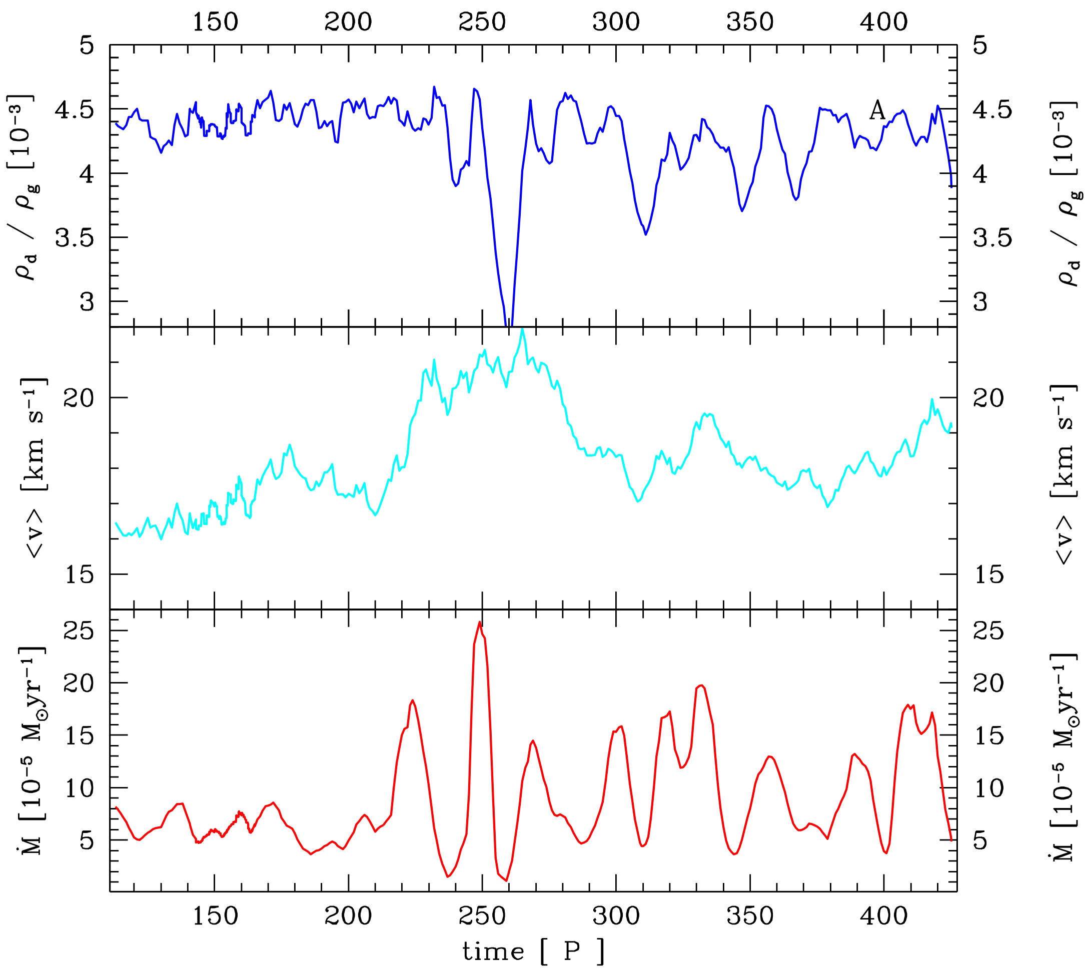

Figure 5: Temporal variation of the mass loss rates of Model A. **Upper diagrma:** the temporal variation of the dust to gas ratio ρ_d/ρ_g, **middle diagram:** the temporal variation of outflow velocity, **lower diagram:** the temporal variation of the local mass loass rates at r= 35 R_*.

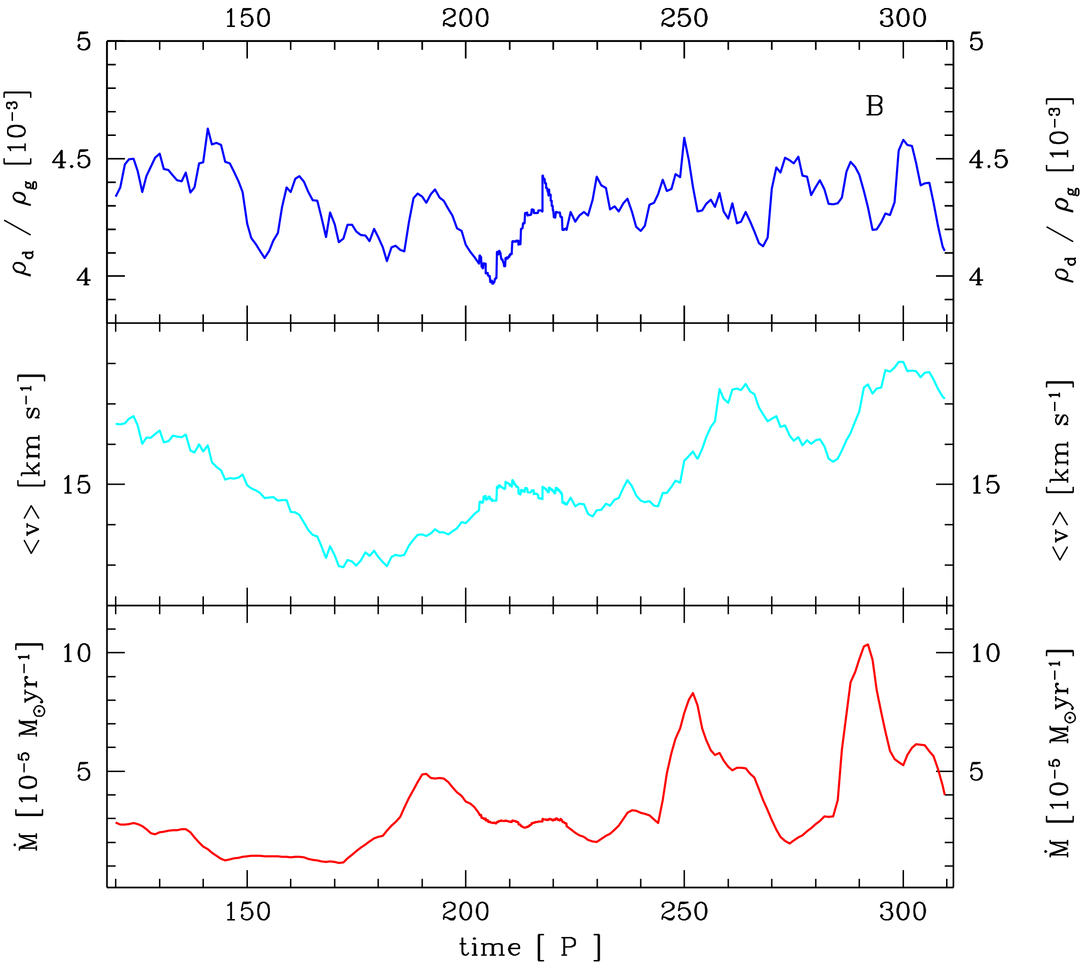

Figure 6: Temporal variation of the mass loss rates of Model B. **Upper diagrma:** the temporal variation of the dust to gas ratio ρ_d/ρ_g, **middle diagram:** the temporal variation of outflow velocity, **lower diagram:** the temporal variation of the local mass loass rates at r= 35 R_*.

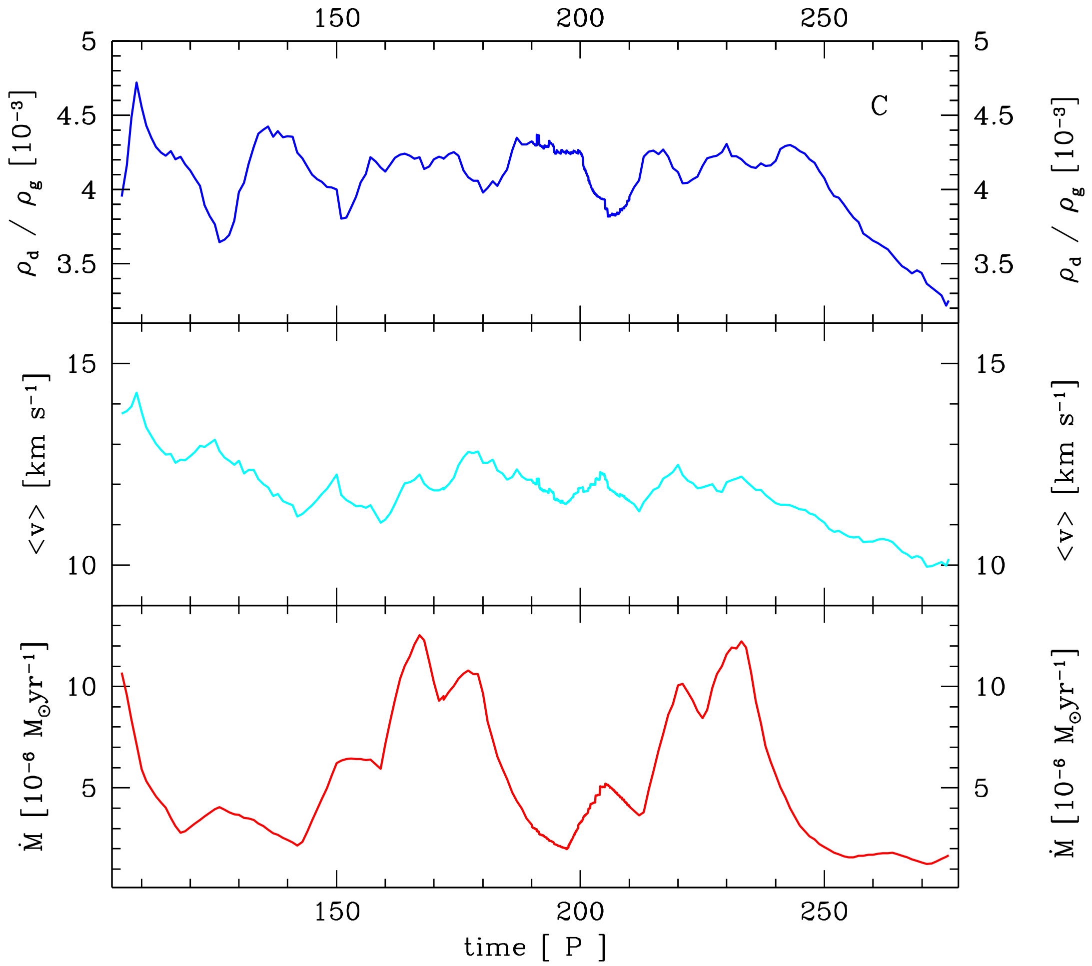

Figure 7: Temporal variation of the mass loss rates of Model C. **Upper diagrma:** the temporal variation of the dust to gas ratio ρ_d/ρ_g, **middle diagram:** the temporal variation of outflow velocity, **lower diagram:** the temporal variation of the local mass loass rates at r= 35 R_*.